JOURNAL OF MATERIALS SCIENCE 33 (1998) 1031–1036

Hot corrosion of chemical vapour deposited SiC and Si_3N_4 in molten Na_2SO_4 salt

D.-Y. SONG, S. KITAOKA, H. KAWAMOTO
Japan Fine Ceramics Center, 2-4-1 Mutsuno, Atsuta-Ku Nagoya, 456 Japan

The corrosion behaviour of SiC and Si_3N_4 prepared by chemical vapour deposition (CVD) technique was investigated in molten Na_2SO_4 salt under argon and argon–oxygen mixture gases. The CVD-SiC was more attacked than the CVD-Si_3N_4 in molten Na_2SO_4 salt. This was in good agreement with the results of the thermodynamic equilibrium calculations. The corrosion of both materials in argon–oxygen mixture was less severe compared to that in argon. This was attributed to the formation of amorphous SiO_2 acting as a protective film against the corrosion. The apparent activation energies of the CVD-SiC and CVD-Si_3N_4 in molten Na_2SO_4 under argon gas were 167 kJ mol^{-1} and 595 kJ mol^{-1}, respectively.

1. Introduction

Silicon carbide and silicon nitride ceramics are potential high temperature structural materials in corrosive environments such as power plant systems and gas turbines because of their excellent high-temperature strength, oxidation and corrosion resistance. Therefore, there have been many studies of the thermal, chemical and mechanical properties of these materials, including the effects of corrosive gaseous environments on their mechanical properties [1, 2]. However, the corrosion behaviour of ceramic materials under molten salt environments is not yet fully understood.

Fox *et al.* [3] investigated the molten salt corrosion of commercial SiC and Si_3N_4 at 1000 °C using a burner rig. They found that the corrosion was proceeded by oxidation to form protective silica scales and the subsequent dissolution of these scales to form non-protective sodium silicates. The chemical corrosion mechanisms were discussed on the basis of acidic/basic dissolution of oxides in molten salts. Tressler *et al.* [4] investigated the corrosion reaction of reaction-sintered and hot-pressed SiC and Si_3N_4 completely immersed in molten salt under air atmosphere. They have shown that the corrosion behaviours depend on the concentration of free oxide ions in the molten NaCl–Na_2SO_4 salts. Mayer and Riley [5] studied the corrosion of reaction-bonded Si_3N_4 by thin films of Na_2CO_3. Initially rapid rates were observed followed by an abrupt slowing of the reaction. Chemical compositions at this slow reaction stage are close to the liquidus on the Na_2O–SiO_2 phase diagram. It thus appears that the accelerated rates are due to formation of sodium silicate liquid and the slow reaction is postulated to be caused by a tridymite layer forming between the melt and Si_3N_4 substrate. Mckee and Chatterji [6] investigated the corrosion of SiC in crucibles and thin films of molten salts. They have shown that rapid corrosion of SiC occurs when the protective SiO_2 layer is attacked by a basic molten salt or a low oxygen pressure is created at the melt/ceramic interface. Jacobson and Smialek [7] have shown that thin films of Na_2SO_4 or Na_2CO_3 lead to thick glassy products on SiC after 48 h at 1000 °C. These products contain small amounts of sodium silicate and 10 to 20 times the amount of silica formed in simple oxidation at 1000 °C over the same time period.

These studies mentioned above are useful to understand the hot corrosion behaviour under molten salt environments. However, all of them have been concerned with commercial SiC and Si_3N_4 formed by addition of sintering promoting additives. Many studies have revealed that the corrosion behaviour are affected by those additives [5, 8–12]. Therefore, it is essential that pure and dense SiC and Si_3N_4 prepared by chemical vapour deposition (CVD) technique are used in studying the inherent nature of corrosion behaviour.

In this study, the corrosion behaviours of highly pure and dense CVD-SiC and CVD-Si_3N_4 in Na_2SO_4 molten salt are investigated under argon and argon–oxygen mixture gases, and the corrosion mechanisms are discussed in relation with the thermodynamic equilibrium calculations.

2. Experimental procedure

The materials used were SiC (α-type) and Si_3N_4 (α-type) without additives, which were fabricated by CVD technique. The specimens were cut to 10 × 10 × 0.5 mm, cleaned ultrasonically in acetone and dried. Fig. 1 shows schematically the apparatus for the corrosion test. In each test, a weighed specimen and powdered reagent grade Na_2SO_4 (about 12 g) were put into a highly pure alumina (>99.5%) crucible. This crucible was placed into a Tamman tube, of highly purified alumina, with 95 mm inner diameter and 600 mm in length, then placed into an electric furnace controlled at a desired temperature. The

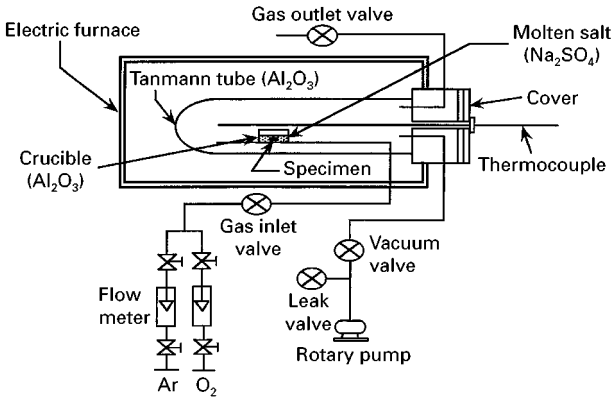

Figure 1 Schematic diagram of the reaction apparatus.

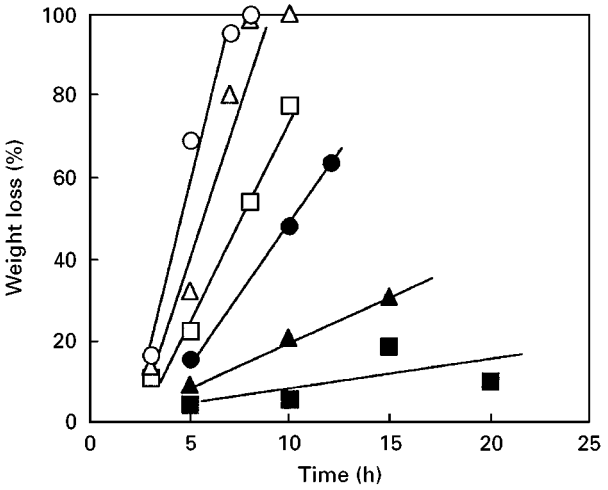

Figure 2 Weight change with time of CVD-SiC ((○) 950 °C; (△) 930 °C; (□) 900 °C) and CVD-Si_3N_4 ((●) 1080 °C; (▲) 1050 °C; (■) 1020 °C) in molten Na_2SO_4 at various temperatures under argon gas.

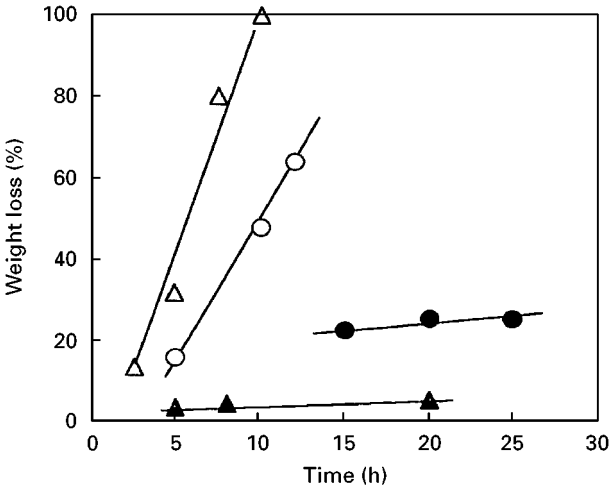

Figure 3 Weight change with time of CVD-SiC and CVD-Si_3N_4 in molten Na_2SO_4 under argon and argon–oxygen mixture gases (CVD-SiC: 930 °C, CVD-Si_3N_4: 1080 °C). CVD-Si_3N_4: (○) Ar; (●) Ar + O_2. CVD-SiC: (△) Ar; (▲) Ar + O_2.

testing temperature of CVD-SiC and CVD-Si_3N_4 was changed from 900 to 1000 °C and from 1000 to 1080 °C, respectively. The time exposed to the molten salt in flowing argon ($\geqslant$ 99.9999%) and argon–oxygen ($\geqslant$ 99.99%) mixture gases was varied from 3 h to 25 h (CVD-SiC: 3 $\sim$ 10 h, CVD-Si_3N_4: 5 $\sim$ 25 h). These conditions were determined on the basis of the results of preliminary corrosion tests, including effect of specimen size. The gases were injected into the Tamman tube at a rate of 10 ml min^{-1}. The total gas pressures were maintained at 1.013×10^5 Pa throughout the tests. The partial pressure of impurity oxygen contained in the argon gas was measured by CP-X type oxygen sensor (NGK Insulators. Ltd.). The oxygen partial pressure of argon–oxygen mixture gas was determined by adjusting the volume ratio of the argon and oxygen gas (0.8 vol% argon–0.2 vol% oxygen).

After the test was completed, the specimen cooled to room temperature was removed from a Tamman tube. The specimen was washed in distilled water at about 80 °C to remove any residual Na_2SO_4 and sodium silicate. The crystalline phases and microstructures on the surface of corroded specimens were examined by X-ray diffraction (XRD) and scanning electron microscopy (SEM).

3. Results and discussion

3.1. Weight change

Fig. 2 shows the weight change with time of the specimens immersed into the molten Na_2SO_4 salt in the temperature range from 900 to 1080 °C under argon gas. The weight loss rate of both CVD-SiC and CVD-Si_3N_4 increased with increasing temperature. The weight loss of specimens also increased linearly with increasing immersing time, that is, this seems to follow a linear rate law, where the reaction is controlled by interface between Na_2SO_4 and ceramic. Moreover, though the testing temperatures of CVD-SiC were lower than those of CVD-Si_3N_4, the CVD-SiC was more severely attacked compared to the CVD-Si_3N_4. It can be said, therefore, that the CVD-Si_3N_4 material was much less reactive in molten Na_2SO_4 under argon gas atmosphere. This is similar to the results reported for commercial SiC and Si_3N_4 by Jacobson and Fox *et al.* [9, 13] and Federer [14]. They suggest that the higher solubility in silicate melts of CO(g) as compared to N_2(g) may lead to faster product escape and more reaction.

Fig. 3 shows the influence of oxygen partial pressure on the weight loss of CVD-Si_3N_4 and CVD-SiC in argon and argon–oxygen mixture gases. The weight loss of both materials under mixture gas (high oxygen partial pressure, $P_{O_2} = 0.202 \times 10^5$ Pa) was significantly lower than that under argon gas (low oxygen partial pressure, $P_{O_2} = 0.1013$ Pa).

This trend is similar to that reported by Mckee and Chatterji [6] for corrosion of SiC in crucibles and under thin films of molten salts. They have shown that rapid corrosion of SiC occurs when the protective SiO_2 layer is attacked by a basic molten salt or a low oxygen partial pressure is created at the melt/ceramic interface.

3.2. Surface morphology

Fig. 4 shows the surface morphologies of the CVD-SiC specimens before and after corrosion under argon

gas. The specimen surface before corrosion is smooth and flat, but the corroded specimen is extremely rough and reveals general pitting, probably caused by the dissolution of the substrate involving gas evolution in molten salt (surface irregularities observed in the Fig. 4 were caused by the severe pitting in localized regions, where oxygen partial pressure was much lower compared to that of the surface). This pitting shows a porous honeycomb-like structure, which is similar to that observed on the SiC substrate surface of corroded α-SiC by Smialek and Jacobson [15]. In the case of CVD-Si_3N_4 the pitting appears somewhat less severe and the substantial grain boundaries are preferentially attacked, as shown in Fig. 5. This trend

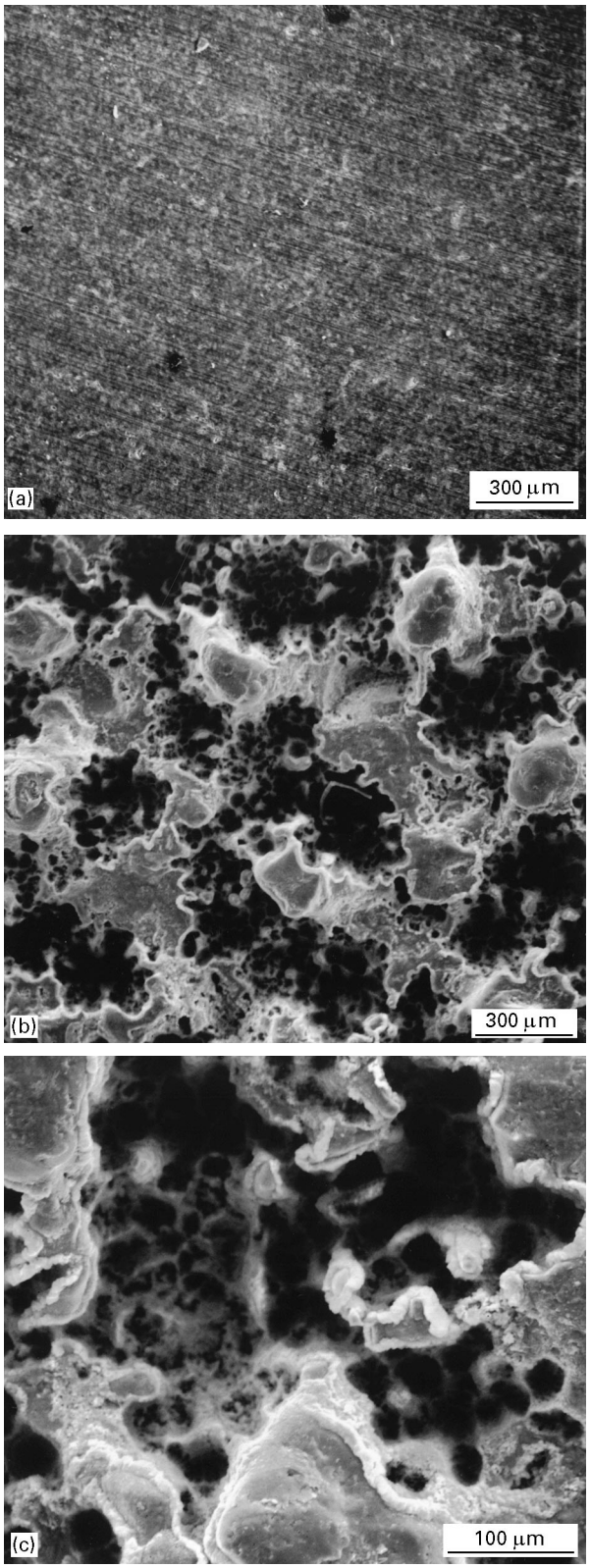

Figure 4 Surface photographs of CVD-SiC before and after corrosion under argon gas: (a) before corrosion; (b) after corrosion at 950 °C for 5 h; and (c) magnified image of region indicated by arrow in (b).

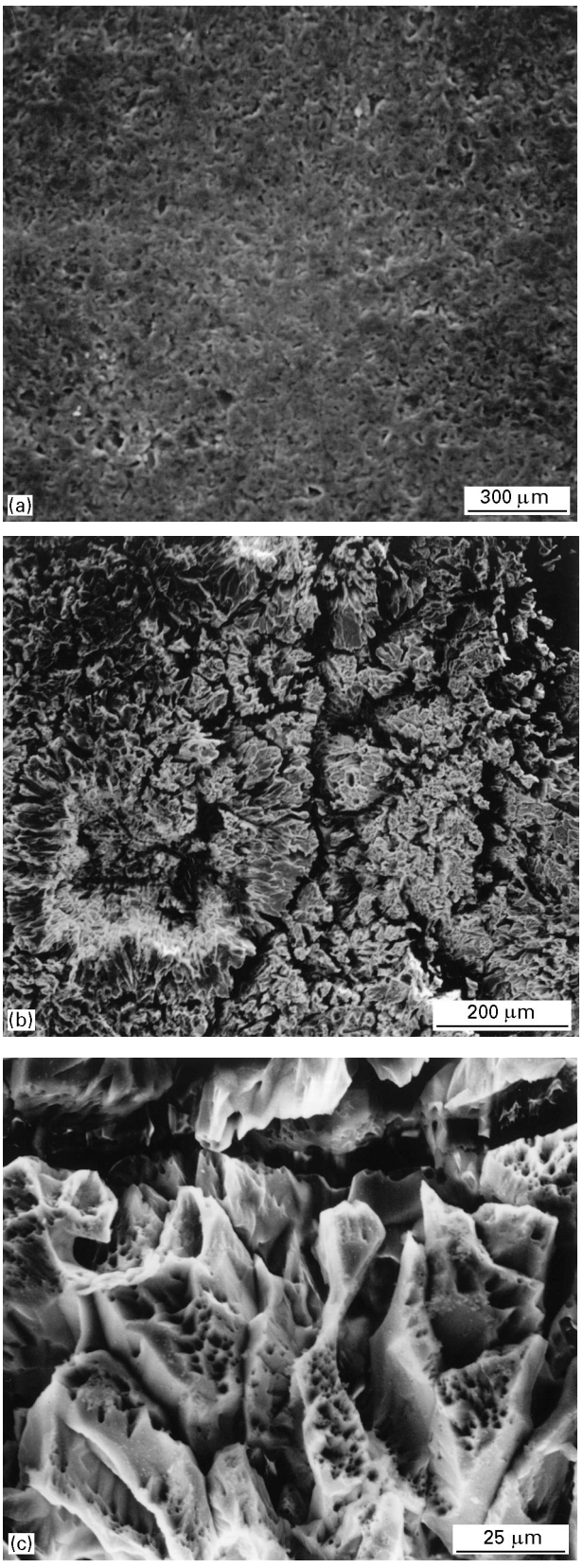

Figure 5 Surface photographs of CVD-Si_3N_4 before and after corrosion under argon gas: (a) before corrosion; (b) after corrosion at 1080 °C for 10 h; and (c) magnified image of region indicated by arrow in (b).

is identical to the results by Jacobson *et al.* [16] who described predominant grain boundary attack of Si_3N_4 as opposed to pitting attack of SiC. Surface morphology of the CVD-Si_3N_4 specimen corroded under argon–oxygen mixture gas is shown in Fig. 6. Corrosion product of white powder was observed on the surface of the corroded specimen after washing in the distilled water (this white powder was also observed on the surface of the CVD-SiC specimen under the same environment).

The change of X-ray diffraction patterns caused by corrosion was not, however, identified for the CVD-SiC and CVD-Si_3N_4. This indicates that no crystalline corrosion products were formed on the specimen surfaces. So it is believed that the white corrosion product formed on the specimen surfaces under argon–oxygen mixture gas is likely to be amorphous SiO_2, which acts as a protective film against corrosion.

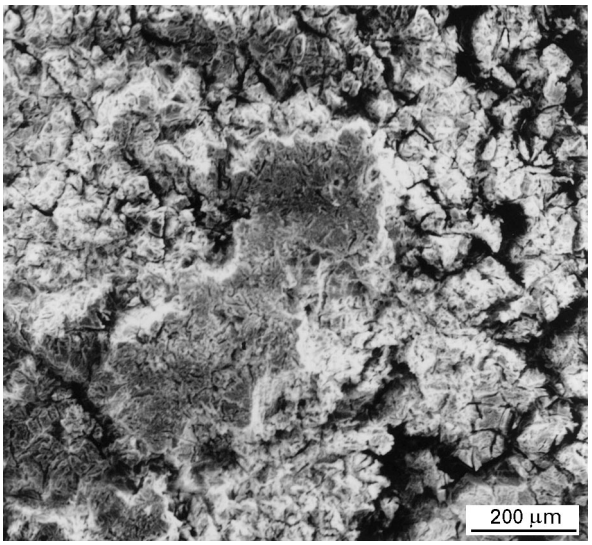

Figure 6 Surface photograph of CVD-Si_3N_4 corroded under argon–oxygen mixture gas.

3.3. Corrosion mechanisms and oxidation rates in molten Na_2SO_4 salt

As mentioned above, the weight loss rate of CVD-SiC in molten Na_2SO_4 salt was faster than that of CVD-Si_3N_4, and the corrosion of both materials under argon was considerably severe compared to that under argon–oxygen mixture. These corrosion behaviour can be characterized by considering the thermodynamic equilibrium calculations (where all thermodynamic equilibrium calculations are obtained using the ChemSage program [17]).

Fig. 7 shows the phase stability diagram obtained by the thermodynamic equilibrium calculations for Na–S–O system. This figure was calculated by using the minimum activity of Na_2O when the following reaction (where $x = 1$) proceeds for various temperatures

$$xSiO_2 + Na_2O(s) = Na_2O{\cdot}x(SiO_2)(l) \qquad (1)$$

It is found that Na_2S is stable when oxygen partial pressure is low (i.e. Na_2SO_4 acts as oxidizer when oxygen partial pressure). Therefore, when dissolved oxygen concentrations in Na_2SO_4 are as low as argon gas atmosphere, it is thought that the oxygen formed by dissolution of Na_2SO_4 leads to the oxidation reaction of SiC and Si_3N_4.

The possible reactions of the oxidation and reduction in the system of SiC, Si_3N_4 and Na_2SO_4 can be expressed as Equations 2 and 3 by the thermodynamic equilibrium calculations

$$2SiC + 2Na_2SO_4 = 2SiO(g) + 2CO(g) + Na_2S \qquad (2)$$

$$Si_3N_4 + 6Na_2SO_4 = 3SiO_2 + 2N_2(g) + 6Na_2SO_3 \qquad (3)$$

Subsequently, the dissolution of SiO_2 and SiO is considered to be favoured thermodynamically as

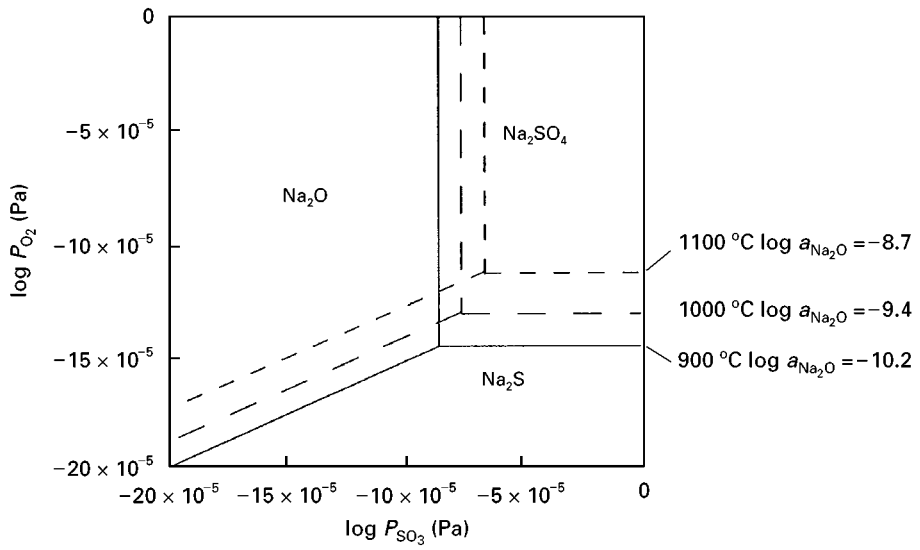

Figure 7 Phase stability diagram for Na–S–O system.

follows

$$SiO_2 + Na_2SO_3 = Na_2O{\cdot}SiO_2 + SO_2(g)$$
$$\Delta G^0 = -57\ \text{kJ mol}^{-1} \quad (4)$$

$$2SiO(g) + Na_2SO_4 = Na_2O{\cdot}SiO_2 + SO_2(g)$$
$$\Delta G^0 = -342\ \text{kJ mol}^{-1} \quad (5)$$

In the case of CVD-SiC, SiO(g), CO(g) and Na_2S are formed by the reaction with Na_2SO_4 and then the gaseous SiO subsequently reacts with the excess Na_2SO_4 and formed the liquid $Na_2O{\cdot}SiO_2$, leading to rapid oxidation–dissolution. While, for CVD-Si_3N_4 the formed amorphous SiO_2 is dissolved by Na_2SO_3 and then acceleration corrosion occurs. Fig. 8 shows the temperature dependence of the thermodynamic equilibrium mole fractions, which is determined by minimizing the Gibbs' free energy, for SiC/Na_2SO_4 and Si_3N_4/Na_2SO_4 system. The calculations were conducted under the presence of excess Na_2SO_4 in order to simulate the actual experimental conditions (i.e. mole ratio: SiC/Na_2SO_4 = 1/10, Si_3N_4/Na_2SO_4 = 1/10). It can be seen that all of the SiC and Si_3N_4 are oxidized under the equilibrium conditions. However, in the SiC system the Na_2S exists in the equilibrium state, but in the Si_3N_4 system the $Na_2O{\cdot}2(SiO_2)$ are formed under 1000 °C instead of forming Na_2S. It is predicted from these results that the molten salt of SiC system is more strongly basic than the Si_3N_4 system. Therefore, it is expected that the SiC is more remarkably corroded than the Si_3N_4 because the corrosion reaction of SiC occurs in the more strongly basic environment compared to the case of Si_3N_4. This trend is in good agreement with the experimental

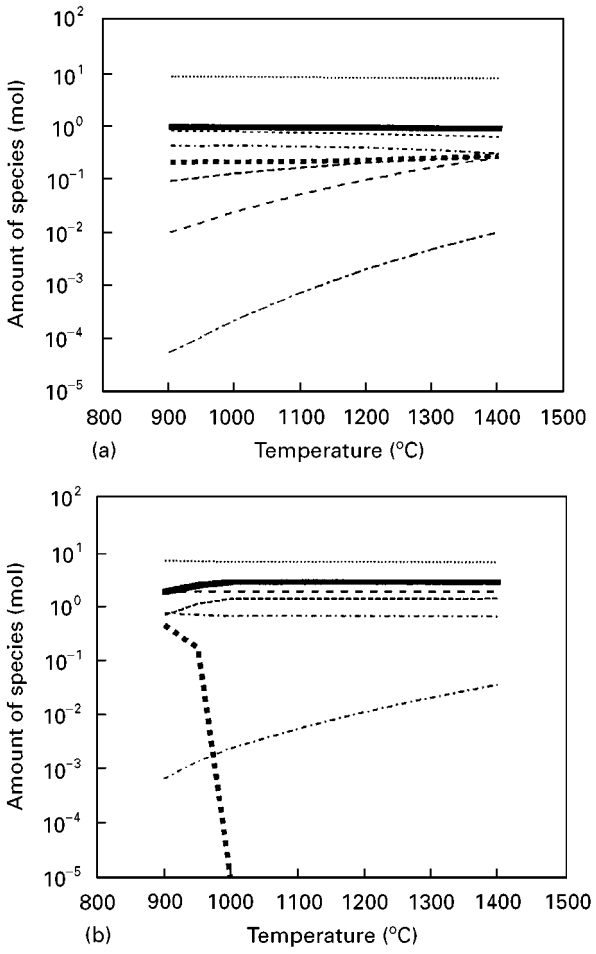

Figure 8 Temperature dependence of thermodynamic equilibrium mole fractions. SiC = 1 mol, Na_2SO_4 = 10 mol, total pressure = 1.013×10^{-5} Pa. (a) (– – –) CO(g); (---) CO_2(g); (–·–) SO(g); (---) SO_2g; (–·–) S_2(g); (···) Na_2SO_4; (——) Na_2SiO_3; (■ ■ ■) Na_2S. (b) (– – –) N_2(g); (–·–) SO(g); (---) SO_2(g); (–·–) S_2(g); (···) Na_2SO_4; (——) Na_2SiO_3; (■ ■ ■) $Na_2Si_2O_5$.

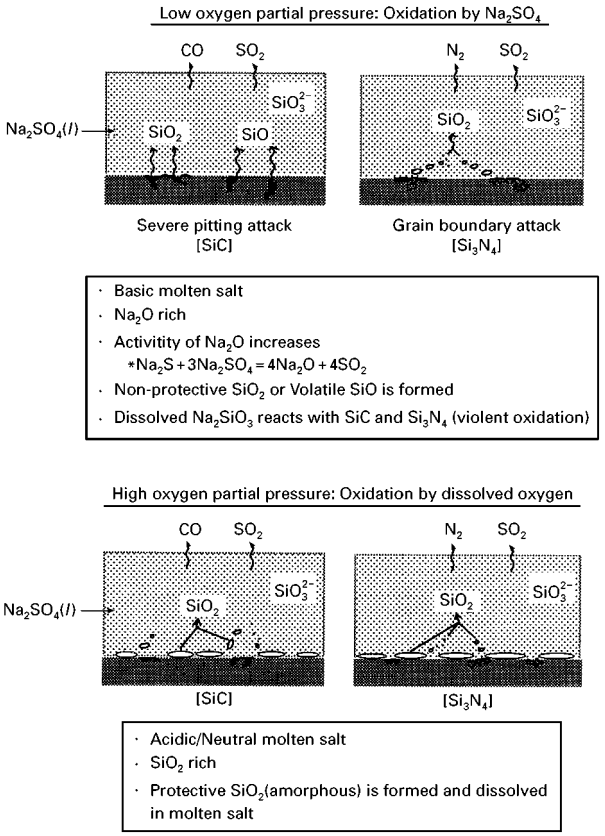

Figure 9 Schematic representation for the corrosion behaviour of CVD-SiC and CVD-Si_3N_4 in the presence of excess molten Na_2SO_4 salt.

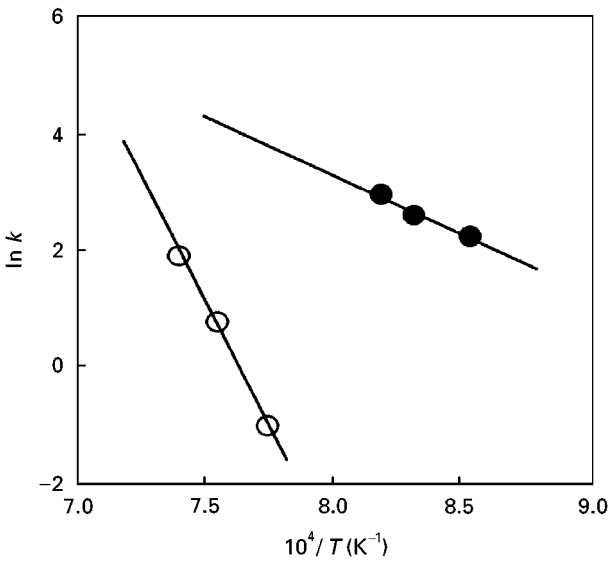

Figure 10 Arrhenius plot for the corrosion rate constants for CVD-SiC in molten Na_2SO_4 salt under argon gas. (●) CVD-SiC, E = 167 kJ mol^{-1}; (○) CVD-Si_3N_4, E = 595 kJ mol^{-1}.

results. These corrosion behaviours of CVD-SiC and CVD-Si_3N_4 in molten Na_2SO_4 salt are summarized schematically in Fig. 9.

Fig. 10 shows Arrhenius plots for oxidation rate of CVD-SiC and CVD-Si_3N_4 in molten Na_2SO_4 under argon atmosphere. This plot of the rate constant k against $1/T$ is linear. These results indicate that the rate of the oxidation is controlled by the direct reaction between these materials and Na_2SO_4 salt. Also, the apparent activation energies of CVD-SiC and CVD-Si_3N_4 were 167 kJ mol^{-1} and 595 kJ mol^{-1}, respectively.

4. Conclusions

The corrosion behaviours of highly pure and dense CVD-SiC and CVD-Si_3N_4 in Na_2SO_4 molten salt were clarified in relation with the thermodynamic equilibrium calculations. The obtained results are as follows:

1. The CVD-SiC was more attacked than the CVD-Si_3N_4 in molten Na_2SO_4 salt. This was good agreement with the results of the thermodynamic equilibrium calculations.
2. Crystalline corrosion products were not identified for both CVD-SiC and CVD-Si_3N_4. For argon–oxygen mixture gas amorphous SiO_2 was formed.
3. The corrosion of both materials in argon–oxygen mixture was less severe compared to that in argon. This was attributed to the formation of SiO_2 acting as a protective film against the corrosion.
4. The apparent activation energies of CVD-SiC and CVD-Si_3N_4 in molten Na_2SO_4 under argon atmosphere were 167 kJ mol^{-1} and 599 kJ mol^{-1}, respectively.

References

1. W. C. BORNE and R. E. TRESSLER, *Ceram. Bull.* **59** (1980) 443.
2. N. S. JACOBSON, J. L. SMIALEK and D. S. FOX, in "Corrosion of advanced ceramics measurement and modelling", edited by K. G. Nickel (Kluwer Academic Publishers, Dordrecht, 1993) p. 205.
3. D. S. FOX, N. S. JACOBSON and J. L. SMIALEK, in "Hot corrosion of silicon carbide and silicon nitride at 1000 °C", Ceramic Transactions **10**, edited by R. E. Tressler and M. McNallan (The American Ceramic Society, Inc., Westerville, OH, 1990) p. 227.
4. R. E. TRESSLER, M. D. MEISER and T. YONUSHONIS, *J. Amer. Ceram. Soc.* **59** (1976) 278.
5. M. I. MAYER and F. L. RILEY, *J. Mater. Sci.* **13** (1978) 1319.
6. D. W. MCKEE and D. CHATTERJI, *J. Amer. Ceram. Soc.* **59** (1976) 441.
7. N. S. JACOBSON and J. L. SMIALEK, *ibid.* **68** (1985) 432.
8. H. WADA and M. YOSHIBA, in "High temperature corrosion of advanced materials and protective coatings", edited by Y. Saito, B. Önay and T. Maruyama (Elsevier Science Publishers B.V., Amsterdam, 1992) p. 355.
9. N. S. JACOBSON and D. S. FOX, *J. Amer. Ceram. Soc.* **71** (1988) 139.
10 H. KAWAMOTO and T. KONDO, *Trans. JSME*(*A*) **58** (1992) 1326.
11. M. LEVY and J. J. FALCO, *Ceram. Bull.* **57** (1978) 457.
12. J. A. COSTELLO and R. E. TRESSLER, *J. Amer. Ceram. Soc.* **64** (1981) 327.
13. D. S. FOX and N. S. JACOBSON, *ibid.*, **71** (1988) 128.
14. J. I. FEDERER, *Adv. Ceram. Mater.* **3** (1988) 56.
15. J. L. SMIALEK and N. S. JACOBSON, *J. Amer. Ceram. Soc.* **69** (1986) 741.
16. N. S. JACOBSON, J. L. SMIALEK and D.S. FOX, in "Handbook of ceramics and composites", edited by N. P. Cheremisinoff (Marcel Dekker, New York, 1990) p. 99.
17. GTT-ChemSage Handbook Ver. 3.0.1, Published by GTT-Technologies, Germany (1994).

Received 30 September 1996
and accepted 5 August 1997